ELSEVIER

Journal of Nuclear Materials 273 (1999) 221–227

journal of nuclear materials

www.elsevier.nl/locate/jnucmat

Diffusion model for the oxidation of Zircaloy-4 at 400°C in steam. The influence of metallurgical structure (precipitates and grain size)

E.A. Garcia [a], G. Béranger [b,*]

[a] *Accidentes Severos, Centro Atómico Ezeiza, Autoridad Regulatoria Nuclear, Avda. del Libertador 8250, 1429 Buenos Aires, Argentina*
[b] *Département de Génie Mécanique, Université de Technologie de Compiègne, LG2mS (UPRES A 6066-CNRS), B.P. 20.529, 60205 Compiègne cedex, France*

Received 13 November 1997; accepted 2 November 1998

Abstract

A model for simulating the oxidation of Zircaloy-4 (Zry-4) in steam at 400°C with different precipitate and grain sizes is presented. The model combines diffusion with interconnecting porosity, defines an interface with discrete propagation in time and is able to reproduce the experimental kinetics. It has been possible in this way to establish a correlation between the parameters responsible for the oxide behaviour (protective or not) and the metallurgical characteristics of the metallic substrate. © 1999 Published by Elsevier Science B.V. All rights reserved.

1. Introduction

The kinetics of high temperature oxidation of Zirconium in an oxidizing gas atmosphere (oxygen, carbon dioxide gas or steam) exhibit successive regimes. The first regimes are in general of parabolic type and later change to 'pseudo-linear' regimes (a series of short parabolic regimes that can be approximated to an average linear regime). Sometimes, only a parabolic regime is observed, after a short initial period related to the establishment of stationary conditions where the kinetics are described as being of cubic type. The transition between the parabolic and linear regimes is described as 'break-away' and is associated with mechanical modifications of the protective scale formed during oxidation. Simultaneously, with the growth of the oxide layer, dissolution of oxygen occurs in the underlying metallic substrate, the α-phase; this oxygen insertion causes brittleness of the oxygen–zirconium solid solution. These two phenomena were intensively studied in terms of diffusion.

The different transitions mentioned above are related to the oxidation conditions (temperature, atmosphere) and to the different metallurgical characteristics of the alloy, as shown in Fig. 1. For oxidation tests on Zircaloy-4 alloy at 400°C in 10.5 Mpa steam, the thermogravimetric curves are all qualitatively similar, but with marked quantitative differences. The transitions are associated with a more or less complex interconnected porosity (InP) perpendicular to the metal surface. It is well-known [1,2] that small pores are generated in the growing oxide scale during the high temperature oxidation of zirconium alloys. The reason why the isolated porosity (IsP) eventually becomes interconnected is not well understood. It may be associated with rapid crack propagation, due to a high stress level in the growing oxide, induced by the volume expansion associated with the formation of the oxide from the metal (the Pilling and Bedworth ratio is 1.56 for the zirconia/zirconium system). However, the oxide is consequently mainly in compression, at least as regards the inner part, and for this reason it is difficult to explain the cracking on this basis. Another possibility is the growth of oxide grains from small grains near the oxide/metal interface to large oriented columnar grains, as the time spent at the oxidation temperature increases [3].

* Corresponding author.

0022-3115/99/$ – see front matter
PII: S0022-3115(98)00691-6

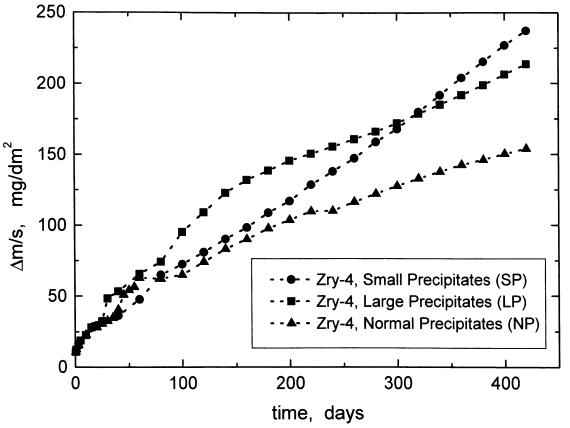

Fig. 1. Experimental oxidation kinetics for Zircaloy-4 at 400°C in steam; with small (SP), large (LP) and normal (NP) precipitate sizes.

Growth of the oxide scale is controlled by the inward diffusion of oxygen through the oxide, the oxidation reaction taking place at the oxide–metal interface. The growth of grains with certain orientations at the expense of others, leading to a textured columnar grain structure, could be the reason for the generation and coalescence of pores in a given direction. The time at oxidation temperature is the reason why InP phenomena are also related to the oxide layer thickness.

The stresses and their effects have been discussed elsewhere, and may have different origins [4]. For example, the stresses can induce phase transformation in the zirconia, which exists in different allotropic forms, such as the tetragonal → monoclinic transition associated with a very large volume change. Several qualitative models have been proposed to describe the cracking and porosity phenomena that produce InP, together with their consequences [5].

This paper presents a diffusion model (Fig. 2), which assumes that a large amount of porosity is generated during initial oxide growth. Possibly due to the time at temperature of each oxide grain created at the oxide/metal interface, some grow at the expense of others and form columnar grains (Fig. 2(a)). At some point, possibly related to the oxide layer thickness or to the number of heating and cooling cycles, the porosity suddenly becomes interconnected (Fig. 2(b)). This fact can be considered by defining a new interface InP/IsP that propagates at high speed. The InP is initiated at the surface when the scale reaches a given thickness propagating in a direction normal to the oxide surface towards the oxide/metal interface. Up to a certain depth in the oxide, at a distance of several microns from the oxide/metal interface, the InP region becomes less protective because of short-circuit paths. The remaining IsP is then the only protective oxide layer. The oxygen concentration gradient in the InP region is very small on average and zero along the interconnecting porosity. In Fig. 2(b), the average gradient is plotted. The InP region is located between ξ_0 and ξ_a with a small average concentration difference $C_1 - C_a$. The IsP region between ξ_a and ξ_1 shows the largest concentration difference in the oxide, $C_a - C_2$. When the remaining IsP region has reached a certain thickness, the interconnecting process restarts (Fig. 2(d)). The mechanism is then repeated, and a new IsP region is developed (Fig. 2(e)). This process will continue up to the break-away represented by a linear behaviour in the kinetic curve. Because this is a continuous gradient in the oxygen concentration profile in the oxide as a function of depth before the break-away (Fig. 2) the total oxide layer IsP + InP becomes substoichiometric. Since the concentration varies from the maximum value C_1 (the only stoichiometric value at ξ_0) to C_2, the minimum substoichiometric value at 400°C, this means that the oxide layer is of the black type.

The purpose of the present paper is to propose a model where the diffusion characteristics are considered but in which the InP phenomena are also taken into account. The aim of this work is to compare the experimental results obtained at 400°C on different Zircaloy-4 substrates to the data calculated by modelling.

The model could also be extended and applied to the case where a simple cracking phenomenon is occurring (as assumed by some authors for describing the 'break away' in terms of mechanical and morphological changes).

2. Experimental procedure

Zircaloy-4 typically contains (Table 1) tin and oxygen which stabilise the α-phase of zirconium and iron and chromium which stabilise the β-phase. Moreover, iron and chromium combine with zirconium to form the intermetallic compound $Zr(Fe,Cr)_2$ [6].

The present work is based on the experimental results obtained by discontinuous testing in an autoclave. To measure the weight gain of the samples at different times, the autoclave cooled down and the samples removed. The successive cooling and heating cycles are able to induce extra stresses between the oxide layer and the metal. However, although this represents an additional disturbing effect in the experiments, these conditions more closely simulate the situation of Zry-4 claddings in a nuclear power plant, with repeated shut downs.

The oxidation kinetics of Zircaloy-4 were studied at 400°C in steam at a pressure of 10.5 Mpa. The samples were previously heated in different conditions in order to obtain different grain and precipitate sizes (Table 2).

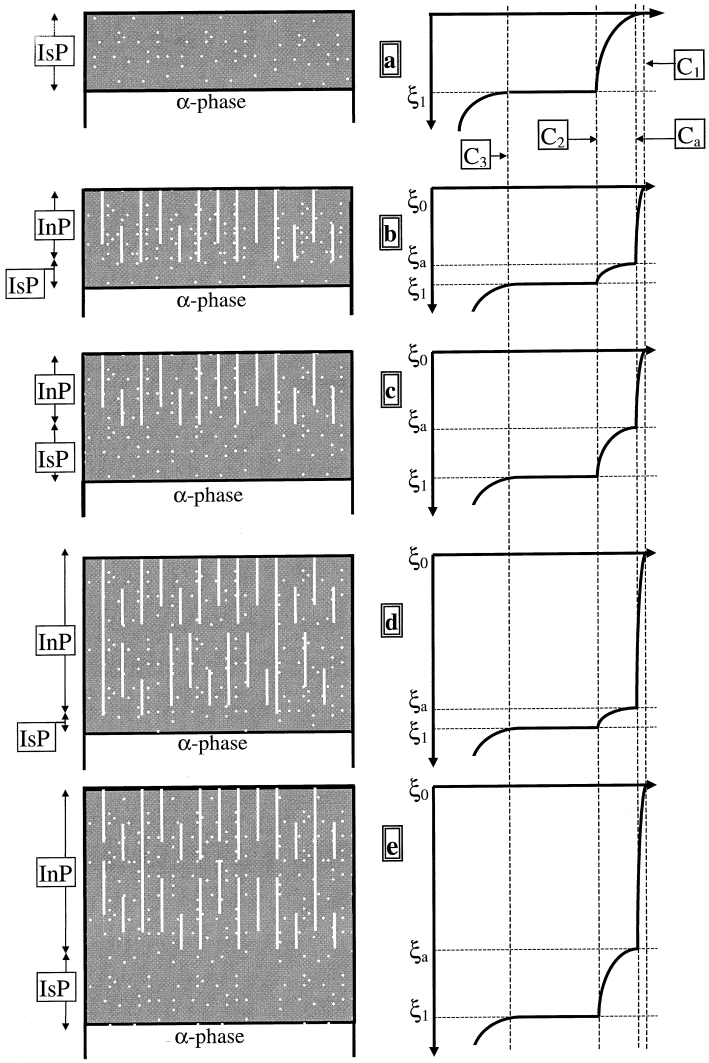

Fig. 2. Successive steps of Zry-4 oxidation. Schematic representation of the proposed simulation model (left), oxygen concentration profile as a function of penetration from the surface (right). For each representation the gas is at the top and the metal at the bottom. (a) First oxide layer formation with IsP (Isolated Porosity). (b) Rapid porosity interconnection up to a certain distance from the oxide/metal interface, defining a region of InP (Interconnecting Porosity) and a certain remaining IsP region. (c) Growth of the IsP region up to a given thickness, the InP region remaining at the same depth. (d) New rapid porosity interconnection up to a certain distance from the oxide/metal interface, defining a large region of InP and a small IsP region. (e) Growth of the IsP region, the new large region of InP conserving constant thickness.

Table 1

Sn (wt%)	Fe (wt%)	Cr (wt%)	O (wt%)
1.2–1.7	0.18–0.24	0.07–0.13	0.08–0.015

3. Diffusion model

To explain the different thermogravimetric results, related to the morphological and structural modifications already mentioned, a simple model is proposed. The model considers both bulk diffusion and short-circuit paths due to a phenomenon that interconnects the oxide porosity [1,7]. To simplify the model, it is considered that the bulk diffusion coefficients in the zirconia layer are not influenced by the phase modifications (allotropic changes).

The short circuit diffusion in the InP region is extremely fast. As a first approximation, in order to simplify the calculation, it is assumed that the concentration $C_a = C_1$ at ξ_a (Fig. 2(b)–(e)). This means that the point where the gas and the oxide are in equilibrium moves

Table 2

Sample	Sample treatment	Precipitate size (μm)	Grain size (μm)
Small precipitates (SP)	Quenched from 1030°C in water then rolled at 500°C	0.03	3 to 5
Normal precipitates (NP)	Recrystallized 3 h at 650°C	0.13	11 to 16
Large precipitates (LP)	Recrystallized 3 h at 650°C and then annealed 50 h at 780°C	0.33	65 to 130

from the external surface into the oxide, Fig. 3. This movement occurs at high speed (10^{-4} cm/s) due to the rapid diffusion once the porosity is interconnected. Consequently, the oxygen flux in the IsP region increases as the InP/IsP interface (ξ_a in Fig. 2) propagates:

$$J^-_{\xi_1^-} = -D^{ox}\left(\frac{dc}{dx}\right)_{\xi_1^-} - \left(\frac{dc}{dx}\right)^{t_a}_{\xi_1^-} < -\left(\frac{dc}{dx}\right)^{t_b}_{\xi_1^-}$$

$$\text{and } -\left(\frac{dc}{dx}\right)^{t_c}_{\xi_1^-} < -\left(\frac{dc}{dx}\right)^{t_d}_{\xi_1^-}$$

then $J_{\xi_1^-}(t_a) < J_{\xi_1^-}(t_b)$ and $J_{\xi_1^-}(t_c) < J_{\xi_1^-}(t_d)$ in the IsP phase, where $t_a < t_b$ and $t_c < t_d$ at the ξ_1 interface (Fig. 2). The oxidation process accelerates, during the extension of the interconnecting porosity associated with a rapid increase in the mass of absorbed oxygen, as it is observed in the rate curve.

The movement of the InP/IsP interface will start at a given time t_i, related to the thickness of the oxide layer and possibly to the number of heating and cooling cycles. At each point when the porosity becomes interconnected, a rapid change in the kinetics curve is observed (Fig. 3(a)). The corresponding times t_i can then be accurately determined from the rate curve. The interconnections will propagate very fast, to a given depth ω_i, leaving a region of oxide thickness d_i, with IsP near the oxide/metal interface. The interconnection process then stops and a new oxidation step starts immediately, generating a new region of IsP growth, with the same mechanism and similar consequences and so on, the phenomenon occurring repeatedly.

For example, Fig. 3(b) schematically shows the oxygen profiles in the case of three steps of InP. This Fig. 3(b) also shows the successive positions of the interface ξ_i, with respect to the oxide/metal interface. Fig. 3(a) shows the corresponding position of ω_i, the interface between oxide with InP and oxide with IsP at the instant t_i when the interconnection process stops. This interface remains stationary up to the instant t_{i+1} when a new interconnection process starts.

With a previously developed code [8], involving solutions of Stefan's multiple interface problem, the kinetic curves were calculated from the present model. There are three types of interface (Fig. 3(b)). The gas/oxide interface, where the concentration is always C_1, corresponds to ZrO_2. The ξ_i interface is a typical Stefan interface, where oxygen mass is conserved through the

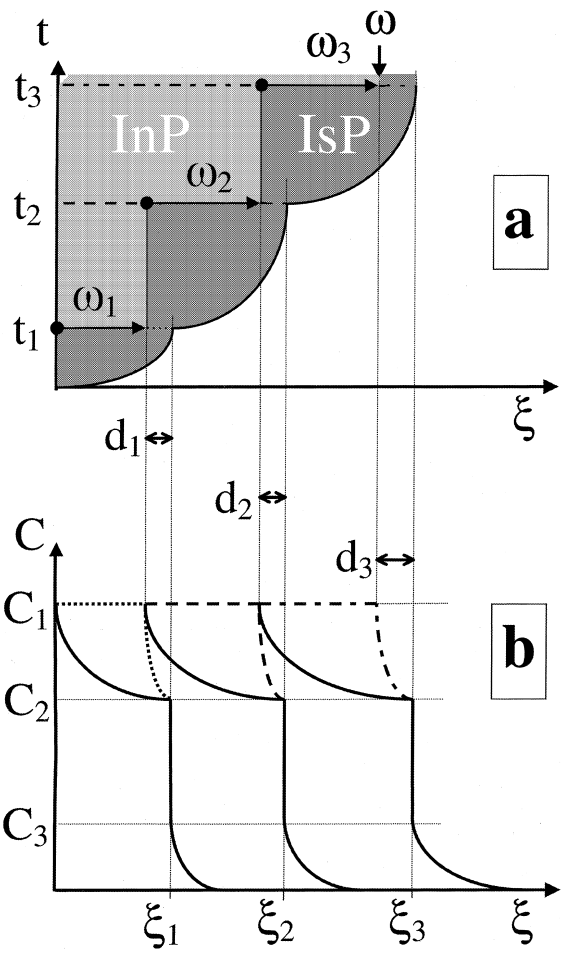

Fig. 3. (a) ξ (oxide/metal interface position) and ω (InP/IsP interface position) vs. t (time): short circuit path development ω_i showing stopping of the InP/IsP interface at (ω_1, ω_2, and ω_3) for times (t_1, t_2, and t_3). At time t_3 the total interconnecting porosity region is $\omega_1 + \omega_2 + \omega_3 = \omega$. (b) C (oxygen concentration) vs. ξ_i (oxide/metal interface position) at different times, t_i: schematic representation of oxidation shown in Fig. 2 where $C_a = C_1$. The minimum thicknesses of the IsP regions (d_1, d_2, and d_3) after the porosity interconnection process at different times (t_1, t_2, and t_3) are shown, together with the corresponding oxide/metal interface positions (ξ_1, ξ_2, and ξ_3) during the repetitive diffusion process.

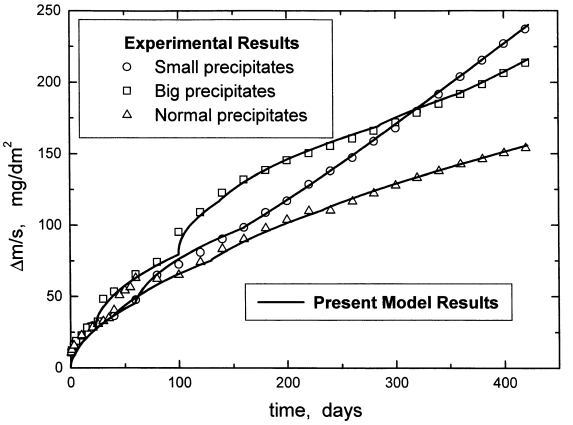

Fig. 4. Comparison between experimental and calculated kinetics.

C_2 to C_3 step. The ω interface, InP/IsP, is the interface corresponding to the average depth of the InP region in the oxide. The oxygen mass does not remain constant across this interface and in this sense it is similar to the gas/metal interface, but with movement inside the oxide.

The input data for the code are:

- Zero velocity for the oxide/metal interface,
- Velocity zero or V for the ω interface, Fig. 3,
- The typical Stefan equation for the ξ_2 interface, for all times, Fig. 2,
- Velocity V of the ω interface when it starts to move, at time t_i,
- The oxygen diffusion coefficients D_i in the oxide phase (IsP) and the α-phase,
- The equilibrium concentrations C_i at the interfaces, for each phase.

The oxygen diffusion coefficients in the oxide, D_{oxide}, and in alpha phase, D_α, and the concentrations at the interfaces C_1, C_2 and C_3, are available in the literature. An approximate value for t_i is obtained from the experimental data.

The fit between the theoretical and the experimental kinetics curves depends on the oxygen diffusion coefficients in the oxide. In the case of the first portion of the curve (first 'parabola'), the same value: $D_0^{\text{ox}} = 1.563 \times 10^{-13}$ cm^2 s^{-1}, was found for the three types of sample. This value differs from that reported for pure zirconia [9] by a factor 0.2. On the contrary, the values of the oxygen diffusion coefficient in the α-phase, D_0^α, and the values of the interface concentrations are the same as those determined for pure zirconium. The low value of the diffusion coefficient, $D_0^\alpha = 1.061 \times 10^{-16}$ cm^2 s^{-1} at 400°C enables it to be considered to be zero in comparison to the oxygen diffusion coefficient in the oxide. The sets of t_i and d_i values then completely define the kinetic curve.

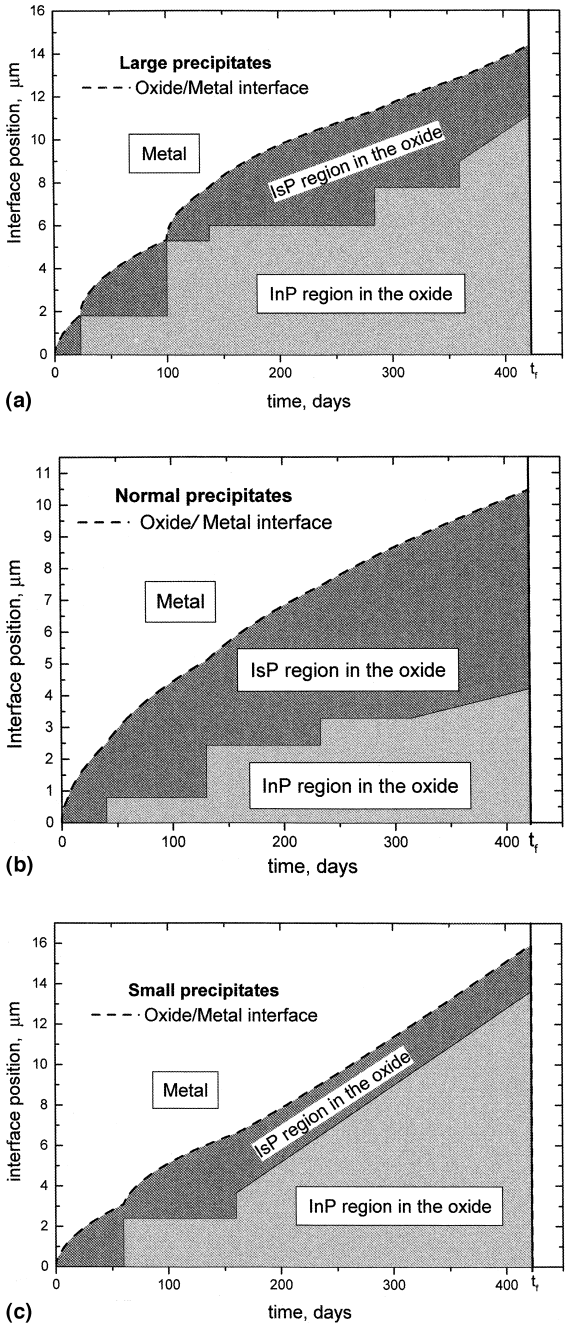

Fig. 5. (a) Metal/oxide interface and InP/IsP interface positions in the case of large precipitate samples (LP). (b) Metal/oxide interface and InP/IsP interface positions in the case of normal precipitate samples (NP). (c) Metal/oxide interface and InP/IsP interface positions in the case of small precipitate samples (SP).

Table 3

Sample type	Precipitate size (μm)	t_i (*d*)	ω_i (μm)	d_i (μm)	100 $d_i/\omega_i + d_i$ (%)	$\omega_i + d_i$ (μm)	Number of cooling and heating cycles
LP	0.33	23	1.8	0.05	23	1.85	4
		100	3.5	0.05	1.4	3.55	2
		137	0.7	1.8	72	2.5	4
		285	1.8	3.6	66	5.4	8
		360	1.2	3.9	77	5.1	4
		360		Linear		–	–
NP	0.13	40	0.8	1.7	69	2.5	5
		130	1.6	2.6	62	4.2	7
		233	0.9	4.1	82	5.0	5
		315		Linear		–	5
SP	0.03	60	2.4	0.6	21	3.0	5
		160	1.3	2.9	70	4.2	5
		160		Linear		–	–

Table 4

Sample type	V (cm/s)
LP	4×10^{-11}
NP	1×10^{-11}
SP	4.4×10^{-11}

4. Results and discussion

The present paper has a dual objective:

- to propose a model with coefficients that can be adjusted to simulate the complex oxidation kinetics of Zircaloy-4 in steam at 400°C,
- to use the model to obtain information concerning the influence of the metallurgical characteristics of Zircaloy-4 on the oxidation kinetics, and especially on the mechanical and physical features of the oxide layer.

The precipitate and grain sizes in the metal are assumed to have no influence on the oxygen diffusion coefficient in the oxide. For this reason, only one oxygen diffusion coefficient D_0^{ox} is imposed for the three experimental kinetics. Fig. 4 shows the kinetics predicted with the present model for the steam oxidation of Zircaloy-4 with either large (LP), normal (NP), or small (SP) precipitate sizes. The comparison between the calculated and experimental results is good, particularly since the experimental data results were obtained from discontinuous, long time test.

The difference between the three rate curves is due to the values of d_i, the minimum distance between the InP/IsP interface and the oxide/metal interface. Fig. 5 shows the positions of the InP/IsP and oxide/metal interfaces as a function of time. The d_i parameter reveals the influence of structure on the mechanical behaviour of the oxide layer. Nevertheless, it can be considered that only the precipitate size has a significant effect on the oxide layer behaviour. In agreement with this consideration, it has been demonstrated by other authors [10], that in oxidation tests performed at 350°C in steam, the oxidation rate is lowest when the precipitates size is larger than 0.1 μm. However, the grain size could affect the diffusion of oxygen along the grain boundaries in the metal; but at 400°C this contribution is very low in comparison to the rate of oxygen diffusion in the oxide, and consequently it can be neglected. The value of the d_i parameter represents the oxide layer thickness not affected by the InP, i.e. the thickness of protective IsP oxide. Table 3 shows the influence of precipitate size, not only on the d_i and ω_i values, but also on the thickness of the IsP layer as a percentage of the total oxide thickness $100d_i/\omega_i + d_i$. This percentage does not change with precipitate size for long oxidation times ($\geqslant 130$ days). On the contrary, for shorter times ($\leqslant 130$ days), the NP samples show a different behaviour to the LP and SP materials. In particular, in the case of the SP sample, the pseudo-linear regime appears at a very early stage.

In the case of the break-away pseudo-linear regime, it is assumed that cracks perpendicular and parallel to the surface dominate the InP phenomenon. The perpendicular cracks propagate continuously, their length increasing linearly with time. This overall linear behaviour in fact involves a series of small increments of InP. Table 4 thus shows the influence of the different precipitate sizes on the interface speed, V, during the linear regime. Once again, the NP samples shows a different behaviour compared to the LP and SP types.

From the experimental results (Fig. 4) it can be seen that the samples are heated and cooled several times from one t_i to the next t_{i+1}. The successive heating and cooling cycles are thus not sufficient to produce a movement of the InP interface; it is also necessary to have a minimum oxide layer thickness. Table 3 summarises the maximum protective oxide layer thickness,

$\omega_i + d_i$, at time, t_i, and the total number of heating and cooling cycles endured by a layer without inducing a change in InP. In a previous work it was shown that a succession of cooling cycles during the experimental test has a significant influence on the oxidation kinetics of Zirconium [11], and of Zircaloy-2 and Zr–2.5 wt% Nb alloy [1].

In a previous Raman spectroscopy study of the tetragonal to monoclinic transition in zirconium oxide [12], the authors show in their Fig. 5 the proportion and position of the different phases. In particular, the monoclinic zirconium oxide phase is situated at the external surface of the scale and grows in steps at each change in kinetics. Comparison with the present results (Fig. 5(a)) clearly reveals a good correspondence between the present InP region and the monoclinic ZrO_2 region determined by these authors [12]. The monoclinic ZrO_2 formed at the external surface of the scale during oxidation is therefore a non-protective oxide. Furthermore, beneath the monoclinic phase these authors [12] mention a tetragonal phase that is in good agreement with the present IsP region. This correlation suggests that the tetragonal ZrO_2 thus becomes the protective oxide in the scale.

5. Conclusions

A model that combines interconnecting porosity (possibly cracking) and diffusion, with an interface separating 'interconnecting porosity and isolated porosity' moving in steps as a function of time, has been developed in order to simulate the complex kinetics observed during the oxidation of Zircaloy-4 in steam at 400°C with successive heating and cooling cycles. The model predicts that the precipitate size in the alloy has a significant influence on the mechanical and morphological evolution of the oxide scale and consequently on its protective nature, producing differences in the resulting kinetics.

It has been shown that the protective IsP oxide region and the non-protective InP oxide region correspond to the tetragonal and monoclinic phases mentioned elsewhere.

Acknowledgements

The authors gratefully acknowledge the collaboration of P. Barberis and D. Charquet from the CEZUS Company who performed the experimental oxidation tests and of J. DAVIDSON for correcting the English.

References

[1] B. Cox, J. Nucl. Mater. 148 (1987) 332.
[2] B. Cox, Y. Yamaguchi, J. Nucl. Mater. 210 (1994) 303.
[3] E.A. García, J. Nucl. Mater. 224 (1995) 299.
[4] J. Godlewski, thesis July 1990, Université de Technologie de Compiègne, France.
[5] L.H. Keys, G. Béranger, P. Lacombe, J. Less-Common Met. 14 (1968) 181.
[6] D. Charquet, R. Hahn, E. Ortlieb, J.P. Gros, J.F. Wadier, Zirconium in the Nuclear Industry, San Diego (1989) STP 1023, p. 405.
[7] F. Lefebvre, C. Lemaignan, J. Nucl. Mater. 248 (1997) 268.
[8] E.A. Garcia, J. Kovacs, J. Nucl. Mater. 210 (1994) 78.
[9] R. Piotrkowski, A. Denis, J. Kovacs, E.A. Garcia, J. Nucl. Mater. 202 (1993) 252.
[10] F. Garzarolli, H. Stehle, Improvements on water reactor fuel technology and utilisation, IAEA, Stockholm, September 1986, p. 387.
[11] J. Com-Nougue, F. Morin, G. Béranger, P. Lacombe, Sonderdruck aus Werkstoffe und Korrosion, September 1972.
[12] J. Godlewski, J.P. Gros, M. Lambertin, J.F. Wadier, H. Weidinger, in: C.M. Eucken, A.M. Grade (Eds.), Zirconium in the Nuclear Industry: Ninth International Symposium, ASTM STP 1132, American Society for Testing and Materials, Philadelphia, 1991, p. 416.